Published in final edited form as:

J Biomed Mater Res B Appl Biomater. 2020 October ; 108(7): 2981–2994. doi:10.1002/jbm.b.34628.

High-throughput 3D bioprinting of corneal stromal equivalents

Shallu Kutlehria[†], **Thanh Cong Dinh**[†], **Arvind Bagde**, **Nilkumar Patel**, **Aragaw Gebeyehu**, **Mandip Singh**

College of Pharmacy and Pharmaceutical, Sciences, Florida A&M University, Tallahassee, Florida

Abstract

In this study we designed high-throughput 3D bioprinting of corneal equivalents which may address the need for in vitro models. In our digital 3D cornea model, average dimensions of adult cornea were converted to 3D shapes, then to G-code files which were printed by BIOX printer (CELLINK). To maintain the curvature of cornea, a support scaffold was designed using stereolithographic printer. The support scaffold could facilitate the printing of 6–12 corneas at a time thus enabling high-throughput printing. Human corneal keratocytes (HCKs) were incorporated in the optimized bio-ink, and cell-laden corneal stromal equivalents were printed. Printed structures were cross-linked by calcium chloride 100 mM, washed with Hanks' Balanced Salt Solution and incubated at 37°C in fibroblast media. Printed corneas were analyzed for live dead assay, Alamar assay, and expression of fibronectin and actin green markers. Printed corneas were able to maintain their structure, integrity, and clarity. Live dead assay and Alamar assay demonstrated that HCKs maintained high viability (>95%) for 2 weeks. HCKs in the printed corneas showed expression for fibronectin and actin green. In conclusion, high-throughput fabrication of 3D printed corneal stromal equivalents using a combination of stereolithography printing, extrusion based printing, and micro-transfer molding techniques was achieved.

Keywords

3D bioprinting; bio-ink; cornea; high-throughput; hydrogel

1 | INTRODUCTION

The human cornea serves as the optical window of the eye and provides one of the first physiological barriers in ocular drug delivery. The cornea is a highly organized structure composed of mainly collagen Type I divided into five distinct layers. The corneal stroma accounts for roughly 80% of total corneal thickness and contains quiescent keratocytes that are activated in response to injury. Current ocular formulations exist to treat corneal abrasion and diseases, but there are limited in vitro models that accurately represent the human cornea both in terms of structure and composition for which they can be tested on. Animal

Correspondence Mandip Singh, College of Pharmacy and Pharmaceutical Sciences, Florida A&M University, Tallahassee, FL 32307. mandip.sachdeva@famu.edu.

† Shallu Kutlehria and Thanh Cong Dinh contributed equally to the study.

CONFLICT OF INTEREST

The authors declare no potential conflict of interest.

models are thus heavily relied upon which may be costly and may not predict human responses in clinical trials accurately. Conventional in vitro models of the human eye are limited in truly mimicking the ocular environment, and the efficiency of fabricating these structures may hinder their utilization for ophthalmic drug development. The cornea serves as a major absorption site for topically delivered ocular drugs, thus in vitro models for delivery screening must be physiologically accurate to predict clinical responses and be capable of high-yield manufacturing. Extrusion-based three-dimensional (3D) “bioprinting” shows prospect in constructing a corneal model that is cost-effective, geometrically accurate, and physiologically relevant for ocular drug development.

3D bioprinting is an additive manufacturing technique in which cells are encapsulated within a “bio-ink” that mimics the native extracellular matrix (ECM) and are subsequently deposited in a layer-by-layer manner to the specified geometry (Sommer & Blumenthal, 2019). This method of tissue fabrication offers unique advantages over traditional 3D in vitro models in the precise tailoring of scaffold structures and the high-throughput automation of generating tissue constructs. The choice of bio-ink material is specific to cell type, with the utilization of synthetic and natural polymers to provide a degradable scaffold that facilitates the growth of cells into viable tissues (Nam & Park, 2018). Extrusion-based bioprinting has demonstrated the feasibility of printing muscle, heart, skin, liver, lung, and corneal scaffolds (Grigoryan et al., 2019; Grix et al., 2018; He et al., 2018; Isaacson, Swioklo, & Connon, 2018; Kim et al., 2018; Noor et al., 2019). The use of this technology shows great prospect in a variety of areas including patient-specific transplantable organs, improved in vitro models, and other biomedical applications. This method of scaffold fabrication enables proliferation and spheroid formation in all directions, unlike traditional 2D monoculture assays (Edmondson, Broglie, Adcock, & Yang, 2014). 2D culture environments may become relevant in the field of tissue engineering because studies have shown that the resulting cell cultures are both morphologically and physiologically different compared to their phenotypes in vivo (Baharvand, Hashemi, Ashtiani, & Farrokhi, 2004). These observations occur due to gene expression and the signal transduction cascade, resulting in cellular responses that may not be predictive of what will occur in the human body. Thus, utilizing a culture system in which cellular response is most accurately recapitulated is highly important in tissue regeneration. In particular, 3D bioprinted culture models have gained increasing recognition for offering more physiologically relevant and predictive data in which pharmaceutical drugs can be screened for in vitro tests. This may allow the utilization of in vitro patient-specific drug testing to reduce the risk of unforeseen adverse reactions and more accurately predict in vivo responses for clinical trials.

The creation of a human corneal stroma equivalent was first achieved through 3D bioprinting of a patient-specific digital model taking a total of less than 10 min to produce (Isaacson et al., 2018). This study demonstrated the feasibility of printing low-viscosity bio-inks with the freeform reversible embedded suspension of hydrogels (FRESH) method on a support scaffold to fabricate corneal structures that are physiologically accurate and facilitate the growth of corneal keratocytes. This method necessitates the use of printing within temporary thermo-reversible gelatin support slurry. This support reagent displays rheological behavior similar to Bingham plastic and can be removed after printing (Hinton et al., 2015). In this study, fused deposition modeling (FDM)–based printing was used to create a support

scaffold to house the gelatin bath and maintain the shape integrity of corneal stroma. In extrusion-based printing of hydrogels or thermo-plastics, the feature resolution of constructs is determined by the nozzle diameter. Although decreasing the nozzle diameter may increase the resolution of the structure when bioprinting, higher extrusion forces are required to extrude the material which has shown to negatively affect cell viability (Emmermacher et al., 2020; Fakhruddin, Hamzah, & Razak, 2018). Micro-transfer molding on the other hand has demonstrated to be a rapid method to fabricate microstructures of high resolution onto collagen Type I hydrogels (Tang, Golden, & Tien, 2004). This method of imprinting consists of a mold with a relief pattern pressed onto a softened or melted polymer layer which can be repeated with low cost, high throughput, and high resolution.

Stereolithography (SLA) printing is another form of rapid 3D prototyping in which a liquid resin is photopolymerized by a UV laser to form a solid object (Sommer & Blumenthal, 2019). This method has shown utility for biomedical applications in printing soft tissues and transplantable devices. A major advantage of SLA printing is that printing can achieve a feature size of 25 μm. This characteristic is particularly emphasized when printing highly curved structures because more layers can be printed, resulting in a more apparent curvature. However, there is no published literature on the bioprinting of corneal structures in conjunction with SLA methods.

Hence, in the current study we combined extrusion-based printing, SLA printing, and micro-transfer molding, and automation to 3D print corneal stroma equivalents with versatile printing parameters and high resolution. We printed support scaffold using SLA printer and created G-code file which would facilitate the rapid bioprinting of 6–12 corneas at a time. We optimized our bio-inks and printing parameters to be utilized with micro-transfer molding via the scaffold apparatus to increase resolution of resulting stromal models.

In this study, we designed a novel approach to 3D bioprinting corneal stroma in tandem with micro-transfer molding, optimized bio-inks with quality by design (QbD) techniques and utilized G-code to replicate tissue models in a high-throughput fashion. Our tissue model was designed taking average dimensions of the adult corneal stroma, converting them to a 3D shape that could be further sliced into G-code, and then printing with a BIO X 3D printer (CELLINK, Gothen-burg, Sweden). A support scaffold was manufactured by SLA printer (Formlabs, Massachusetts) to help maintain the curvature of the cornea during printing and to mold high-resolution features that would be difficult to achieve by extrusion alone. This support scaffold could facilitate high-throughput printing of 6–12 corneas and enabled using bio-inks of optimized mechanical properties to minimize printing time.

2 | MATERIALS AND METHODS

2.1 | Materials

Sodium alginate (MW 50000 Da) and gelatin Type B from bovine skin (MW ~50,000–100,000 Da), calcium chloride analytical grade, and anti-fibronectin antibody were purchased from Sigma Aldrich (St Louis, Missouri). Human corneal keratocyte (HCK) cells and fibroblast media were purchased from ScienCell (Carlsbad, California). NucBlue fixed cell stain ready probes reagent was purchased from Invitrogen (Thermo Fischer Scientific,

Massachusetts) and Actin green 488 ready probes reagent was purchased from Thermo Fischer Scientific. Live-Dead assay reagent/viability Assay Kit was purchased from Biotium Inc. Anti-rabbit Texas and FITC secondary antibodies were purchased from Santa Cruz Biotechnology. Polylactic acid (PLA) (Lulzbot TAZ 6, Colorado), SLA printer Form 2, Clear Resin, and Dental SG Resin (Formlabs) and Alamar blue dye (Invitrogen, California). Type I bovine collagen solution-Fibricol was purchased from Advanced BioMatrix.

2.2 | Preparation of digital stroma model

The dimensions of the stroma were taken from average measurements of human adults and were digitally modeled in Autodesk Fusion 360 with a central thickness of 500 μm, periphery thickness of 700 μm, uniform radius of 5.80 mm, and a sagittal height of 3.0 mm. These measurements were sketched onto a plane then revolved about the y-axis to create a 3D stromal shape. A stereolithography file (STL file) was then generated which could be later converted to G-code.

2.3 | Generation of G-code

The corneal STL file was converted to G-code utilizing the Slic3r software. A concentric printing pattern was chosen with a set printing origin of the bottom center of the corneal well. A layer height of 200 μm was chosen with a 25% infill density. This file was then converted to G-code in Repetier-Host to quality check printing movements, missing artifacts, and replication of a digitally accurate model. G-code to print 6 or 12 corneas was prepared by introducing nonextrusion movements to navigate between adjacent wells. After printing the first cornea, the printhead was programmed to rise out of the well by 10 mm and move sequentially in the X direction to the next well of a given row. Once the last cornea of a row is printed, the printhead raises and moves in the Y direction to a new row to begin printing in the reverse X direction. The overall path to print 12 corneas followed a serpentine fashion as shown in Figure 1e. This served as our template code to which parameters such as temperature, print speed, extrusion pressure, and activation of a second printhead to dispense crosslinking agent could be varied.

2.4 | Preparation of high-throughput corneal support scaffold

A support apparatus, on which the stroma would be printed upon, was prepared by inscribing our corneal model within a 56 mm × 42 mm × 6 mm rectangular prism so that the scaffold would complement the anterior surface of the corneal model. This resulted in a concavity, which we will call a corneal well; it helped to maintain the ocular dimensions of the cornea during printing. The corneal well also contained a small dead volume to accommodate adding crosslinking agent after printing. These well patterns could be repeated along the rectangular prism in uniform rows to the desired number of corneas. A 6- and 12-well scaffold was initially FDM printed with PLA using a 22G nozzle. We then utilized an SLA printer Form 2 (Formlabs) for printing the support scaffold with Clear Resin (Formlabs) and Dental SG Resin. The layer height for the Clear and Dental SG Resins was 25 and 50 μm, respectively. The corneal supports were positioned at different angles with respect to the build plate to modify the tessellation pattern on the surface of the corneal wells. Aligning the support parallel to the build plate resulted in parallel concentric circles.

Supports were created with a touchpoint size of 0.6 mm using the Auto-Generate tool with the PreForm software.

2.5 | Preparation and optimization of Bio-Ink

Sodium alginate, gelatin Type B, and Type I bovine collagen solution-Fibricol 10 mg/ml were used to prepare the bio-ink. Briefly, gelatin was dissolved in 0.45% wt/vol NaCl solution by heating (40°C in water bath) and intermittent vortexing for 1 hr. Sodium alginate was added to the above solution followed by the addition of FibriCol to the sodium alginate/gelatin gel. Thereafter, using 0.1 N NaOH solution, the pH was adjusted to 7.0. Osmolality was adjusted to 295–300 mOsmol/kg by using sodium chloride. The final gel was sonicated to remove the air bubbles.

Bio-inks were developed using the Box–Behnken design. To assess the effect of different variables, 12 design points and 5 center points were chosen. Gelatin concentration (A), alginate concentration (B), and temperature (C) were selected as independent variables while optimizing the bio-ink. Ten bio-inks containing varying percentage of sodium alginate, gelatin, and collagen were prepared to conduct further testing (Table 1). Optimization was founded on the tan (delta) which is the ratio of loss modulus (G′′) to storage modulus (G′). Statistical calculations were done by Design Expert 7.0.0. (Stat-Ease Inc., Minnesota).

2.6 | Rheology testing

The rheological behavior of the gels was investigated by comparing the flow curves of each ink using an AR1500ex rheometer (TA instruments, Dallas, Texas) with a 20-mm parallel plate geometry and a gap height of 1,000 μm. The inks were melted at 37°C in a water bath for 10 min before being poured onto the plate and subsequently cooled to 4°C to reach a steady state. Excess gel was scraped before conducting tests. Oscillation temperature ramps for the inks were performed from 4 to 40°C with a ramp rate of 5°C/min and constant angular frequency of 10.0 rad/s. Samples were taken at 10 s/pt with a 1% strain. Loss moduli (G′′), storage moduli (G′) along with the loss tangent (tan delta) were determined for each ink with increasing temperature (data not shown). The temperature at which the loss modulus is equivalent to the storage modulus was chosen as an initial estimate for their ideal printing temperature. Flow sweeps for the gels were performed at the temperature at which (G′′) = (G′) to see the shear thinning profiles of the inks. A shear rate of 1.0–100.0 1/s was applied with averaging time and an equilibration time of 30.0 and 5.0 s, respectively.

2.7 | Light transmission examination

Corneal bio-ink as well as corneal transparency was evaluated by using a microplate reader to examine light transmittance as outlined by previous studies (Kim et al., 2019). Bio-ink was melted at 37°C and pipetted into a 48-well plate to reach a height of 500 μm to match the thickness of the human cornea. 3D printed corneas were also placed in the wells of same plate. Light absorbance values were taken from the range of 300–700 nm and light transmittance (T) values were calculated from the light absorbance values (A) described by the following equation: $T(\%) = 1/10^{A} \times 100$. All the transmittance values were corrected by taking into consideration the absorbance of blank as reference.

2.8 | Acellular optimization of printing parameters of corneas

An SLA-printed cornea using clear resin was used as a simple model to compare our bioprinted corneas before further characterization. A precise, concentric printing pattern was chosen in order to ensure adhesion of previous layers in the Z direction during extrusion to facilitate an optically clear construct.

A desktop bioprinter BIO X (CELLINK) with piston-driven syringe heads and pneumatic printheads was used for printing. UV sterilization system of BIO X was used to sterilize the environment during the printing. The high-throughput printing of corneas was possible by creating a G-code file that contained 12 corneas along with a defined print path to navigate between each well. After printing the first model, the code was designed to raise the printhead out of the well by 10 mm and move sequentially in the X direction to the next well of a given row. The overall path to print 12 corneas followed a serpentine fashion as shown in Figure 1e. This served as our template code to which parameters such as temperature, print speed, extrusion pressure, and activation of a second printhead to dispense crosslinking agent could be varied.

Optimizing an individual ink proceeded by selecting temperatures at which the loss tangent ranged between 0.25 and 0.45. The first cornea was printed at the lowest temperature in this range, and the subsequent printing temperature was increased by 1°C utilizing a temperature-controlled printhead (CELLINK) between each cornea. A 10-min delay was programmed before proceeding to the next well in order to allow the inks to reach equilibrium temperature. The extrusion pressure was also decreased to prevent smearing of scaffold structure. Nozzles were also replaced between each print to ensure that residual gel of the previous temperature was not printed with. A similar method was utilized to print six corneas using the support scaffold as shown in Figure 1c.

After printing, 200 μl of 100 μM calcium chloride ($CaCl_2$) was added to each cornea, and they were allowed to crosslink for 3 min. Thereafter, $CaCl_2$ was removed and corneas were washed with Hanks' Balanced Salt Solution (HBSS) three times, removed from the scaffold, and placed in fibroblast media.

2.9 | Characterization of support scaffold and printed corneas

2.9.1 | Scanning electron microscopy for structural characterization of corneas—To observe the features that would be imprinted from the support scaffold onto the resulting corneas, polydimethylsiloxane (PDMS) corneal substitutes were prepared by mixing silicone elastomer base (Sylgard) to silicone elastomer curing agent (Sylgard) in a ratio 10:1 followed by centrifugation to remove air bubbles. The PDMS solution was poured into the support scaffolds until the full volume of the well was reached. The support scaffolds along with the PDMS were placed in an oven for 12 hr at 9°C. The PDMS corneas were then removed from the corneal wells by spatula. After mounting the PDMS sample on the scanning electron microscope (SEM) stub, Pt was sputter-coated about the cornea to avoid charging. SEM images were taken by Helios G4 UC (Thermofisher Scientific) with low acceleration voltage of 2 kV.

2.9.2 | Atomic force microscopy of corneas—To obtain local surface morphology and elastic modulus information of the printed corneas, atomic force microscopy (AFM) was used. We used a Multimode 8 (Bruker, California) with a Nanoscope V controller. A CONTAu high-density carbon cantilever with spherical tip of radius 30 ± 5 nm and spring constant of 0.2 N/m used in ScanAsyst mode was gifted by the NanoandMore USA, California, was used. A scan rate of 1 Hz was chosen over a square scan size of 10 μm. Data were collected over three different surfaces on the printed corneas with height information in 3D with a scan size of 25 μm. Rq and average of absolute values of surface height deviations measured from the mean plane (Ra) were also measured. In order to hold corneas securely while performing studies, we designed and SLA-printed cornea holder using SG Dental resin (Figure 5e). The holder comprised of a cornea seat (Figure 5a,c) and cornea seat lid (Figure 5b,d) The cornea seat had dimensions of (14 × 14 × 3.5 mm (length, width, height) with a dome diameter 10 mm and height of 3 mm at the center of the block for the cornea to rest on. The cornea lid was fitted to match the outside curvature of 3D printed cornea with a hole in the middle to exposed 1 mm in sagittal height of the cornea during AFM testing. The cornea was securely placed on the cornea seat. Cornea lid was then placed on the cornea and AFM was performed. The cornea was kept moist during the study by adding HBSS on top of the cornea.

2.9.3 | Bright-field microscopy for comparison of corneal scaffold—Different wells of SLA-printed scaffolds were compared to assess the variation in the radius at different regions using Keyence wide area 3D measurement system VR series (Illinois).

2.9.4 | Characterization of corneal dimension—Printed corneas were evaluated for diameter, central thickness, and peripheral thickness using Vernier calipers (General tools and Instruments, New Jersey). The dimensions falling within range 1% of mean values were used for the studies.

2.10 | Printing with HCK cells

HCKs were Passage 2–7 and were mixed with Ink 2 at concentration of 3.0×10^6 cells/ml and printed using a BIOX printer. Printed corneas were placed in fibroblast media supplemented with fibroblast growth factors, 5 mM $CaCl_2$, penicillin, and fetal bovine serum. Media was changed every other day.

2.10.1 | Evaluation of corneas for cell viability—Cell viability was assessed at Days 1, 7, and 14 using live dead assay. Briefly, the cover media of the printed corneas was removed and the corneas were washed with HBBS three times. Live and dead assay solution was prepared by mixing the calcein and ethidium bromide II in a ratio of 1:4. Live/dead assay staining solution was directly added to corneas to submerge them. The plate was incubated for 30 min at 37°C. Corneas were viewed under fluorescent microscope (Olympus 1×71) using Texas red and FITC filter. Cell viability was calculated by using the image J1.51K software (NIH). RGB images were converted to binary images to analyze the cell number by counting particle number. Percentage viability was obtained by using equation: (number of live cells/total cells [both live cells + dead cells]) × 100.

2.10.2 | Evaluation of cell growth—Alamar blue assay was used to assess the cell number/growth over the period of time. In brief, the corneas were washed with HBSS, 10% Alamar blue dye was added to the wells containing corneas. The plates were incubated at 37°C, 5% CO_2 for 4 hr. Furthermore, 100 μl media from each well was collected and added to the 96-well plate. The fluorescent intensity at excitation wavelength 560 nm, emission wavelength 590 nm, and absorbance at 570 nm was observed by plate reader (Tecan, Austria). The procedure was repeated on Days 1, 10, and 14.

2.10.3 | Immunofluorescence staining to evaluate expression of F-actin and fibronectin biomarkers—The printed corneas were also evaluated for expression of actin green and fibronectin. Briefly, corneas were washed with HBSS. Cells in the corneas were fixed using formaldehyde (4%) for 30 min. Permeabilization was done using 0.1% triton X-100 for 30 min. After washing with HBBS, the cells were incubated with primary antibody fibronectin (Sigma) 1:200 for overnight. Texas red conjugated secondary antibody was added, and corneas were incubated for 3–4 hr. NucBlue fixed cell stain ready probes reagent (Invitrogen, ThermoFisher Scientific) and Actin green 488 ready probes reagent to label phalloidin (Thermo Fisher Scientific) were added to the wells and incubated at 37°C (30 min). The corneas were observed with a fluorescent microscope using DAPI, FITC, and Texas Red filter.

2.11 | Statistical analysis

The experiments were carried out in triplicates. Data were expressed as mean ± standard deviation. Statistical differences were evaluated by analysis of variance (ANOVA) Bonferroni's multiple comparison tests. The p value ($p < .05$) was set as criterion for statistical significance.

3 | RESULTS

3.1 | Cornea and support scaffold creation

Digital cornea model was designed to facilitate printing of 3D cornea (Figure 1a, b). Cornea model accommodated for curvature, variable central, and peripheral thickness, as well as diameter and overall shape resembling the normal human stroma (Figure 1g). The support scaffold due to triangulated tessellation enabled printing of smooth, uniform, and optically clear corneas.

3.2 | Optimization of bio-ink and 3D printing

Bio-ink was finalized by using three independent variables: gelatin concentration (A), sodium alginate concentration (B), and temperature (C). Tan (delta) was documented for 17 runs, and analysis was performed by using ANOVA (Table 2). The data were found to behave like a quadratic model. Linear and higher cubic model were aliased for tan (delta) (Tables 2 and 3).

From ANOVA, A, C, AC, BC, B^2, and C^2 variables significantly affected the tan (delta). This suggested that gelatin concentration and temperature had quadratic effect, whereas alginate concentration had a linear effect (Figure 3a, b). It also suggested that BC and AC

were two-way interactions. Gelatin concentration and temperature showed significant ($p < .0001$) effect on tan (delta) value of the bio-inks. As gelatin concentration was increased, tan (delta) was significantly ($p < .0001$) decreased. Also, as the temperature was increased, tan (delta) was significantly ($p < .0001$) decreased. However, increase in the sodium alginate concentration did not show significant effect on tan (delta) (Figure 3b). Furthermore, in our preliminary printing trials with various bio-inks, it was observed that increasing sodium alginate to 3.25% imparted more stiffness which retained the curvature and shape. Hence, all the responsible factors were developed within the limits selected for design matrix creation. Constraints were applied to acquire minimum tan (delta) values and sodium alginate concentration as 3.25% wt/vol (Table 4). Optimization of bio-ink was also based on the desirability function ranging from zero to one; where zero for the worst response parameters and one for the best response parameters (Figure 3c). The batch showing maximum desirability was chosen for model response prediction and was compared to the results obtained. Thereafter, the optimized bio-ink was repeated (three times), and comparison was performed with predicted responses. No significant differences were observed among the predicted and experimental values as predicted tan delta was 0.31 and experimental value was 0.29. Finally, the optimized bio-ink containing 3.25% wt/vol sodium alginate and 4% wt/vol gelatin in combination with collagen (Ink 2) was printed at a temperature range of 23–24°C and a pressure range of 14–18 kPa. The structures printed with this composition were stiff enough to hold both the curvature and shape while printing. This was mostly due to mechanical properties of sodium alginate, gelatin, and collagen. The bio-ink containing sodium alginate below 3.25% wt/vol and gelatin below 4.0% wt/vol were easily extruded through the printer but were fluid and not able to retain the shape of the corneas. Also, Ink 2 did not cause any needle blockade, clumping even after the incorporation of the cells and led to continuous printing of 6–12 corneal structures. Furthermore, after cross-linking with $CaCl_2$, the corneas were easily detachable without any sticking to the support scaffold or chipping of the edges. Importantly, corneas retained their concave shape in the medium without any twisting or folding around the edges. Also, the corneas were completely transparent (Figure 1h). Transparency was imparted due to the addition of optimum ratio of sodium alginate, gelatin, and collagen as increased concentration of collagen led to reduction in transparency due to its property of becoming opaque on polymerization. In addition, the bio-ink was prepared and mixed with the cells in the manner to minimize the incorporation of the air bubbles. Air bubbles instigate a multitude of problems during printing, that is, needle blocking, excess pressure requirement, and nonuniformity in printed structure. It also affects the cell growth and proliferation.

3.3 | Rheological behavior of bio-inks

In order for material to be extruded, the apparent viscosity should be both low enough to allow easy extrusion while high enough to be stackable on sequential layers. Viscosity was plotted against increasing shear stress to determine the elastic and storage modulus of the formulations (Figure 2a). Printing at temperatures higher than 37°C resulted in the melting of gelatin and a loss in storage modulus of the bio-ink. Temperatures lower than 20°C resulted in using a higher pressure needed to extrude the filament and thus exerting more force on the cells which is not desirable. Oscillation temperature ramps of each bio-ink allowed us to find their respective optimal printing temperature due to the ratio between

storage and loss moduli. The flow sweep tests showed that our gels displayed shear thinning behavior (Figure 2b). This was beneficial in the extrusion process because the gels could flow more easily when pressure was applied. The reduction in viscosity is also beneficial to reduce shear stresses experienced by the cells, which has also shown to be positive for cell viability.

3.4 | Light transmission examination

Transparency of bio-ink (INK2) and 3D printed cornea was evaluated by their ability to absorb or scatter the wavelengths in visible light region (300–700 nm). Transparency was compared to that of water. Water being transparent transmitted most of the light in a wavelength range of 400–700 nm (visible region). Transmittance of Ink 2 as well as 3D printed corneas was observed as 75–90% (Figure 2c).

3.5 | Characterization of printed corneas

3.5.1 | Scanning electron microscopy—SEM of PDMS corneas offered insight to the structure of printed corneas due to a shared imprinting caused from the corneal well. The SLA-printed support allowed the corneas to have an anterior surface resolution of up to 25 μm (Figure 4a,b) as opposed to a maximum resolution of 160 μm when relying on nozzle gauge alone as described in other studies (Isaacson et al., 2018).

3.5.2 | Atomic force microscopy—AFM allowed us to have further insight of Young's modulus of elasticity and surface roughness induced by the SLA-printed supports (Figure 5f,g). The elastic modulus of 3D printed corneal stroma was observed as 42.03 kPa ± 7 at a minimum force ranging from 139.2–147.3 nN. The surface roughness was quantified by root mean square (RMS/Rq) and Ra which were determined at a surface area of 100 μm^2 to be 6.68 ± 0.6 nm and 3.27 ± 0.4 nm, respectively.

3.5.3 | Bright-field microscopy for comparison of corneal scaffold—Bright-field images were captured for two different wells on the same scaffold to confirm the radius of the well and variation between two wells. The data demonstrated that the radius of the well was about 6.5 mm and variation between two wells was 50 μm at the peripheral edges and 30 μm at the center of the corneal structures (Figure 4c).

3.5.4 | Characterization of corneal dimension—Corneal dimensions were observed as 11.6 ± 3 mm diameter, 550 ± 30 μm central thickness, and 700 ± 45 μm peripheral thickness as determined by bright-field microscopy.

3.6 | Evaluation of cell viability

Live dead assay showed the percent cell viability was 96 ± 5% and 86 ± 2% on Days 1 and 14, respectively (Figure 6a, b). Alamar assay also demonstrated that cells maintained their viability and growth in printed corneal scaffold for 2 weeks. Cell growth rate was calculated as percentage of growth on Day 1. Growth rate was observed as 101 ± 9% on Day 5, 98.5 ± 13% and 93.8 ± 7% on Day 10 and Day 14, respectively (Figure 6c).

3.7 | Expression of F-actin and fibronectin

In general, F-actin is predominately distributed in cortical regions near the plasma membrane in the normal corneal keratocytes, and fibronectin is present in ECM promoting cell–cell and cell–matrix adhesions. Printed corneal stromal scaffolds showed expression for F-actin (green) (Figure 6e) and fibronectin (red) (Figure 6d). Owing to the presence of sodium alginate and overall stiffness of gel, the cells did not regain their stellate shape while present inside the cornea. The keratocytes expressed globular morphology as supported by the distribution of F-actin and fibronectin.

4 | DISCUSSION

Extrusion-based 3D bioprinting has demonstrated to be a viable method of tissue fabrication in which cells can grow, proliferate, and recapitulate cellular function within a tailored hydrogel matrix. This process of layer-by-layer deposition enables the rapid production of tissue constructs that mimic the native extracellular environment and physiological structures present in vivo. The feasibility of bioprinting a corneal stroma within a gelatin slurry using the FRESH method has been demonstrated earlier by Isaacson et al. (2018). However, possibilities of gelatin slurry binding to various ECM proteins such as fibronectin and other polysaccharides to leave residual gelatin integrated into the final printed structure have been reported (Hinton et al., 2015). In this study, we propose for the first time a novel high-throughput approach to develop corneal stromal models by optimizing bio-ink printability with gelatin, generating G-code that enables the rapid production of corneas, and printing within a corneal support fabricated by SLA printer. These modifications resulted in (Sommer & Blumenthal, 2019) an improvement in rheological and mechanical characteristics of our collagen-based gels, (Nam & Park, 2018) faster production of corneal models by enabling versatility of printing parameters, and (Kim et al., 2018) an increase in anterior corneal surface resolution.

Collagen Type I was chosen as a crucial component for our formulated bio-inks due to its excellent biocompatibility, natural adhesion epitopes, and high concentration within the corneal stroma (Akhmanova, Osidak, Domogatsky, Rodin, & Domogatskaya, 2015; Massoudi, Malecaze, & Galiacy, 2016). However, collagen by itself may be difficult to use as a bio-ink because of its low viscosity and limited repertoire of crosslinking agents. Thus, we incorporated gelatin Type B to our collagen-based gels, to enhance their rheological characteristics (Guillén, Giménez, López Caballero, & Montero, 2011). However, gelatin displays opposite temperature behavior to collagen that enables it to solidify at lower printing temperatures. In addition, sodium alginate was added to impart mechanical strength and the ability to crosslink and form desired structure on adding $CaCl_2$. However, these parameters alone are not sufficient to optimize printability.

QbD approach has widely been utilized in product/formulation optimization and designing (Bagde et al., 2019; Bagde, Patel, Kutlehria, Chowdhury, & Singh, 2019). It provides significant benefit in terms of systematic evaluation of individual variables and their interactions toward a predefined goal. Design Expert is an important statistical tool to evaluate various constituents used during application of QbD concepts. It helps in optimizing composition by giving maximum information with minimum numbers of

experimental runs. Hence, we used Box–Behnken design to optimize components of our bio-ink. As per our knowledge, this is the first report for applying design expert–based Box–Behnken design to optimize the composition of bio-ink to be used for printing corneal stromal equivalents. Several bio-ink combinations of gelatin/alginate/collagen (Ink 1–Ink 10) were prepared, and oscillation temperature ramps were conducted at a range of 4–40°C to investigate storage and loss modulus, loss tangent, and viscosity. Collagen concentration was kept maximum (5 mg/ml) as was achievable by our optimum gel preparation method. Gelatin and sodium alginate were chosen as independent and tan (delta) as optimum criteria in the design. A previous study of gelatinalginate bio-inks outlined a systematic approach to evaluate and define pneumatic printability based on rheological parameters (Gao et al., 2018). They observed that the storage (G') and loss (G'') moduli were important considerations in quantifying extrudability, uniformity of extrusion, along with the integrity of structure. They found that a ratio of loss (G'') and storage (G') moduli, also known as the loss tangent, between 0.25 and 0.45 resulted in smooth, uniform lines that were optically clear. Our design suggested that gelatin demonstrated to influence the thermosensitivity of the gels more than alginate indicated by the range of tan (delta) values when changing concentration and temperature (Figure 3). This observation is supported by a previous research involving the thermosensitive properties of gelatin hydrogels (Chang, Xiao, & Tang, 2009). We also observed that increasing the gelatin concentration of our bio-inks, while keeping collagen concentration and temperature constant, resulted in a higher storage modulus. The improved mechanical properties observed by the addition of gelatin demonstrated to be desirable for printing. A flow sweep test of gel was then conducted at their respective printing temperatures to evaluate their viscosity at increasing shear forces. The rheology time sweep plots of viscosity vs shear rate as well as plot of shear rate vs shear stress demonstrated shear thinning properties of Ink 2. Ink 2 had higher viscosity as compared to other inks which ensured no smearing and consistent printing at pressure of 14–18 kPa. The addition of gelatin to our inks resulted in corneas with sufficient mechanical integrity to be printed while maintaining accurate corneal dimensions.

As the ultimate goal for fabricating corneas was to develop high-throughput in vitro screening model which enables fast screening of various formulations, excipients, as well as experimental conditions, high-throughput printing of corneas was must in order to obtain sufficient number of corneas for the studies in least amount of time. To facilitate rapid production of corneal models, a support scaffold and G-code must be prepared with the desired number of corneas. While designing corneal support scaffold as well as cornea model, we took into consideration patients' corneal dimension including radius, central thickness, peripheral thickness, and saggital height. Saggital heights of human cornea have been reported to be ranging from 3.14 to 4.04 mm (Sorbara, Maram, Fonn, Woods, & Simpson, 2010). It has also been reported that the saggital height of anterior cornea depends upon central corneal curvature, degree of asphericity, diameter of cornea, as well as the curvature of paralimbal sclera (Young, 1992). Furthermore, direct bio-printing onto the support scaffold must be possible while maintaining geometric accuracy of the original model, and high-speed processing and removal of these corneas must be possible. To achieve these parameters, we relied on using a support scaffold fabricated by SLA printing because of its increased resolution when compared to FDM printing. This is due to SLA printing

relying on the polymerization of a resin via a laser to form a 3D construct with increased resolution, whereas FDM printing resolution is highly limited by the nozzle diameter. Decreasing the nozzle diameter allows for more resolution with features but requires more pressure for the filament to be extruded.

Molding techniques employ the use of a liquid-like filament to retain the inner shape of an encapsulated rigid substrate. The gelatin elastic component of the hydrogels promoted support of layer-by-layer extrusion, while the alginate and collagen viscous components allowed slight molding to our SLA-printed support scaffold. The SLA-printed support scaffold had a high resolution of 25 μm which had not been achieved by previous FDM-printed corneal supports (Isaacson et al., 2018). Also, this resulted in a cornea with high curvature and smoothness due to fusion of deposited layers against the SLA-printed interface. However, high reproducibility, uniformity, thickness, and curvature could not have been achieved if microtransfer molding technique was not used in conjugation with 3D bioprinting technology. When corneas were created using only molding technique, the structures were nonuniform, with variable thickness and deformed curvature. Furthermore, optimizing the rheological balance between elastic and viscous portions was performed by comparison between G' and G''. These gels could still maintain their shape fidelity as demonstrated by characterization of the thickness and diameter of the printed corneas. This was highly desirable in our goal of developing a high throughput system in which corneal constructs could be printed. Efficiency of corneal printing was further enhanced by generating a support scaffold and G-code that could print 6–12 corneas at a time. The fusion of deposited layers demonstrated improved optical clarity, enabling limited defraction of light between sequential layers. Corneal structures were optically clear and stretchable after crosslinking. The corneas were able to maintain their storage modulus in the fibroblast media containing 5 mM $CaCl_2$. It has been reported that human cornea is nearly transparent and absorbs about 20% of incident light at 400 nm (Van Best, Bollemeijer, & Sterk, 1988). The transmittance of 3D printed corneas was observed as 75–90% at 400–700 nm wavelength, which was comparable to literature values (Ramamurthy et al., 2015).

We performed SEM analysis of PDMS corneas to confirm their structural and surface characteristics in order to characterize the support scaffold. As such, it was not feasible to perform AFM analysis of either directly printed corneas (due to their soft texture) or SLA-printed support scaffold due to size issues. Hence, we designed PDMS corneas using same support scaffold which was used while printing corneas. SEM analysis showed uniform concentric impressions with height resolution of 25 μm on the corneas which was possible due to the aligning of SLA scaffold parallel to build plate. We were also able to achieve an enhanced layer height resolutions of 50 and 25 μm in corneal scaffolds by using Dental SG resin and Clear resin, respectively. Young's modulus of elasticity of 3D printed corneal stroma was observed as 42.03 kPa ± 7. Our results were comparable to observations reported in the literature. Last, Thomasy, Croasdale, Russell, & Murphy (2012) reported that elastic modulus of human corneal stroma ranged from 24 to 39 kPa and compared consistency of force curves of anterior stroma with that of a soft elastic material. RMS/Rq and Ra of 3D printed corneal stroma (at a surface area of 100 μm^2) were 6.68 ± 0.6 nm and 3.27 ± 0.4 nm, respectively. Lombardo et al. reported Rq values at 10 μm^2 as 102 ± 7 nm and Rq values 70–180 nm at 5 μm^2 in femto-second laser and mechanical cut human stromas (Lombardo, De

Santo, et al., 2012; Lombardo, Lombardo, et al., 2012). It has been reported that surface roughness being the relative parameter is largely affected by the surface area chosen (Jumelle et al., 2017). Furthermore, deviations in 3D printed corneas and literature values may be plausible due to various factors, for example, material and type of probe used during microscopy as well as composition of hydrogel vs real corneal tissue.

The surface and size of printed corneas was determined by the size of each well of SLA-printed support scaffold. Hence, different wells of the support scaffold were compared. Very slight variations (30–50 μm) were observed among different wells suggesting minimal batch-to-batch variation among different scaffolds. Furthermore, dimensions of printed corneas were diameter 11.6 ± 3 mm, central thickness 550 ± 30 μm, and peripheral thickness 700 ± 45 μm, which are very near to that of reported values of human corneas. Literature shows that average horizontal corneal diameter in adults is 11 mm while vertical diameter is 12 mm; central thickness is 470–580 μm and peripheral thickness of human corneas is about 660 ± 76 μm (Martola & Baum, 1968; Mashige, 2013; Ventura, Böhnke, & Mojon, 2001).

Despite opting various strategies to overcome challenges related to 3D printing intricate structures resembling human tissues/organs, the major concern is how cells are retaining their viability, growth, and proliferation in those structures. In fact, cell interactions and different behaviors are influenced by their ECM. ECM components are essential for regulating cell growth and differentiation (Nam & Park, 2018). Therefore, ECM-derived components such as gelatin, fibronectin, agarose, collagen, and hyaluronic acid have been used widely in bio-inks. Hence, collagen, gelatin, and sodium alginate were primary components of our bio-ink. Collagen Type I was chosen as a crucial component due its excellent biocompatibility, presence of natural RGD motif adhesion sites, and high concentration within the corneal stroma. Wu et al. (2016) demonstrated the use of HCK cell-laden scaffolds using sodium alginate (1% wt/vol), gelatin (10% wt/vol), and collagen (0.82 mg/ml)-based ink. In other study, Isaacson et al. (2018) printed corneal stromal scaffolds using methacrylated collagen (8 mg/ml) and sodium alginate (3% wt/vol). However, we optimized bio-ink with collagen 5 mg/ml, gelatin 4% wt/vol, and sodium alginate 3.25% wt/vol. High initial cell viability was observed in our bio-ink which was possible due to the optimal composition of collagen, gelatin along with pressure applied, and nozzle size. Also, cell viability was maintained for up to 2 weeks, after bioprinting the corneal scaffolds. It has been reported that alginate lacks bioactive molecules leading to reduced cell proliferation rate (Das et al., 2015; Derby, 2008). However, adding collagen and gelatin made the constructs more fibrous and offered more binding sites thus making it more suitable for cell growth.

Fibronectin is a extracellular glycoprotein and helps in cell–cell and cell–matrix adhesions. It has been reported to be abundantly present in corneal fibroblast and helps in healing and adhesion (Gordon, 2014). The presence of F-actin and fibronectin in stromal constructs confirmed that cells did not lose their phenotypic markers and maintained their characteristics during printing. Pereira, Sousa, Barrias, Bártolo, & Granja (2018) had shown the expression of fibronectin and actin green in 3D printed biomimetic skin tissues. It was also observed that the cells exhibited round disc-like morphology and formed some clusters. Similar observations have been reported in earlier studies by Ouyang, Yao, Chen, Na, & Sun

(2015)) and Hunt, Smith, Gbureck, Shelton, & Grover (2010) in HEK293FT cell-laden hydrogels and fibroblast-laden hydrogels, respectively. Usually when cells are encapsulated in alginate-based hydrogels, they influence mechanical stiffness of alginate for only a short period of time. However, on longer incubation, alginate retains its integrity thus preventing the cells for gaining original morphology. All our studies demonstrated proof of concept for high-throughput printing of corneal stromal scaffolds which are highly reproducible, mimic human eye in curvature, are transparent, and support cell growth for 2 weeks. However, further studies in terms of optimization of bio-ink, which allows enhanced cell–cell and cell–matrix interactions, and supports cell morphology, along with the creation of top layers supporting corneal epithelial cells, need to be validated for successful translation into real cornea-like structures.

5 | CONCLUSION

Taken together, we designed a model for high-throughput 3D printing and established proof of concept for the feasibility of rapid printing of corneal stromal scaffolds. Due to the optimum ratio of collagen, gelatin, and sodium alginate in the bio-ink, the printed corneas were transparent, smooth, possessed desired curvature, and also supported the growth of HCKs for 2 weeks. This study offers a novel avenue for optimization and design of highly organized and biomimicking structures in integration with composition and component design to obtain 3D printed tissues on large scale.

ACKNOWLEDGMENTS

We would like to thank Dr. Eric Lochner for helping us with AFM studies and Florida State University, Department of Physics, for allowing us to use their facilities. The research was supported by the National Institute on Minority Health and Health Disparities of National Institutes of Health under Award number U54 MD007582 (U54 RCMI grant) and NSF-CREST Center for Complex Materials Design for Multidimensional Additive Processing (CoManD) award # 1735968.

Funding information

NSF-CREST Center for Complex Materials Design for Multidimensional Additive Processing (CoManD), Grant/Award Number: 1735968; the National Institute on Minority Health and Health Disparities of National Institutes of Health, Grant/Award Number: U54 MD007582

Abbreviations:

3D	three dimensional
AFM	atomic force microscopy
ANOVA	analysis of variance
ECM	extracellular matrix
FDM	fused deposition modeling
FRESH	freeform reversible embedded suspension of hydrogels
G′	storage moduli
G′′	loss moduli

HCK	human corneal keratocyte
PDMS	polydimethylsiloxane
PLA	polylactic acid
QbD	quality by design
Ra	average of absolute values of surface height deviations measured from the mean plane
RMS	root mean square
SEM	scanning electron microscope
SLA	stereolithography

REFERENCES

Akhmanova M, Osidak E, Domogatsky S, Rodin S, & Domogatskaya A. (2015). Physical, spatial, and molecular aspects of extracellular matrix of in vivo niches and artificial scaffolds relevant to stem cells research. Stem Cells International, 2015, 1–35.

Bagde A, Patel K, Kutlehria S, Chowdhury N, & Singh M. (2019). Formulation of topical ibuprofen solid lipid nanoparticle (SLN) gel using hot melt extrusion technique (HME) and determining its anti-inflammatory strength. Drug Delivery and Translational Research, 9, 816–827. [PubMed: 30924025]

Bagde A, Patel K, Mondal A, Kutlehria S, Chowdhury N, Gebeyehu A, … Singh M. (2019). Combination of UVB absorbing titanium dioxide and quercetin nanogel for skin cancer chemoprevention. AAPS PharmSciTech, 20(6), 240. [PubMed: 31250221]

Baharvand H, Hashemi SM, Ashtiani SK, & Farrokhi A. (2004). Differentiation of human embryonic stem cells into hepatocytes in 2D and 3D culture systems in vitro. International Journal of Developmental Biology, 50(7), 645–652.

Chang Y, Xiao L, & Tang Q. (2009). Preparation and characterization of a novel thermosensitive hydrogel based on chitosan and gelatin blends. Journal of Applied Polymer Science, 113(1), 400–407.

Das S, Pati F, Choi Y-J, Rijal G, Shim J-H, Kim SW, … Ghosh S. (2015). Bioprintable, cell-laden silk fibroin–gelatin hydrogel supporting multilineage differentiation of stem cells for fabrication of three-dimensional tissue constructs. Acta Biomaterialia, 11, 233–246. [PubMed: 25242654]

Derby B. (2008). Bioprinting: Inkjet printing proteins and hybrid cell-containing materials and structures. Journal of Materials Chemistry, 18(47), 5717–5721.

Edmondson R, Broglie JJ, Adcock AF, & Yang L. (2014). Three-dimensional cell culture systems and their applications in drug discovery and cell-based biosensors. Assay and Drug Development Technologies, 12(4), 207–218. [PubMed: 24831787]

Emmermacher J, Spura D, Cziommer J, Kilian D, Wollborn T, Fritsching U, … Lode A. (2020). Engineering considerations on extrusion-based bioprinting: Interactions of material behavior, mechanical forces and cells in the printing needle. Biofabrication, 12(2), 025022. [PubMed: 32050179]

Fakhruddin K, Hamzah MSA, Razak SIA, editors. Effects of extrusion pressure and printing speed of 3D bioprinted construct on the fibroblast cells viability IOP Conference Series: Materials Science and Engineering; 2018: IOP Publishing.

Gao T, Gillispie GJ, Copus JS, Pr AK, Seol Y-J, Atala A, … Lee SJ (2018). Optimization of gelatin–alginate composite bio-ink printability using rheological parameters: A systematic approach. Biofabrication, 10(3), 034106. [PubMed: 29923501]

Gordon SR (2014). Fibronectin antibody labels corneal stromal collagen fibrils in situ along their length and circumference and demonstrates distinct staining along the cell and stromal interfaces of Descemet's membrane. Current Eye Research, 39(3), 312–316. [PubMed: 24144005]

Grigoryan B, Paulsen SJ, Corbett DC, Sazer DW, Fortin CL, Zaita AJ, … Miller JS (2019). Multivascular networks and functional intravascular topologies within biocompatible hydrogels. Science, 364(6439), 458–464. [PubMed: 31048486]

Grix T, Ruppelt A, Thomas A, Amler A-K, Noichl B, Lauster R, & Kloke L. (2018). Bioprinting perfusion-enabled liver equivalents for advanced organ-on-a-chip applications. Genes, 9(4), 176.

Guillén G, Giménez B, López Caballero M, & Montero GP (2011). Functional and bioactive properties of collagen and gelatin from alternative sources: A review. Food Hydrocolloids, 25, 1813–1827.

He P, Zhao J, Zhang J, Li B, Gou Z, Gou M, & Li X. (2018). Bioprinting of skin constructs for wound healing. Burns & Trauma, 6(1), 5.

Hinton TJ, Jallerat Q, Palchesko RN, Park JH, Grodzicki MS, Shue H-J, … Feinberg AW (2015). Three-dimensional printing of complex biological structures by freeform reversible embedding of suspended hydrogels. Science Advances, 1(9), e1500758.

Hunt N, Smith AM, Gbureck U, Shelton R, & Grover L. (2010). Encapsulation of fibroblasts causes accelerated alginate hydrogel degradation. Acta Biomaterialia, 6(9), 3649–3656. [PubMed: 20307693]

Isaacson A, Swioklo S, & Connon CJ (2018). 3D bioprinting of a corneal stroma equivalent. Experimental Eye Research, 173, 188–193. [PubMed: 29772228]

Jumelle C, Hamri A, Egaud G, Mauclair C, Reynaud S, Dumas V, … Thuret G. (2017). Comparison of four methods of surface roughness assessment of corneal stromal bed after lamellar cutting. Biomedical Optics Express, 8(11), 4974–4986. [PubMed: 29188095]

Kim H, Park M-N, Kim J, Jang J, Kim H-K, & Cho D-W (2019). Characterization of cornea-specific bioink: High transparency, improved in vivo safety. Journal of Tissue Engineering, 10, 2041731418823382.

Kim JH, Seol YJ, Ko IK, Kang HW, Lee YK, Yoo JJ, … Lee SJ (2018). 3D bioprinted human skeletal muscle constructs for muscle function restoration. Scientific Reports, 8(1), 12307. [PubMed: 30120282]

Last JA, Thomasy SM, Croasdale CR, Russell P, & Murphy CJ (2012). Compliance profile of the human cornea as measured by atomic force microscopy. Micron, 43(12), 1293–1298. [PubMed: 22421334]

Lombardo M, De Santo MP, Lombardo G, Lomoriello DS, Desiderio G, Ducoli P, … Serrao S. (2012). Surface quality of femto-second dissected posterior human corneal stroma investigated with atomic force microscopy. Cornea, 31(12), 1369–1375. [PubMed: 22262224]

Lombardo M, Lombardo G, Carbone G, De Santo MP, Barberi R, & Serrao S. (2012). Biomechanics of the anterior human corneal tissue investigated with atomic force microscopy. Investigative Ophthalmology & Visual Science, 53(2), 1050–1057.

Martola E-L, & Baum JL (1968). Central and peripheral corneal thickness: A clinical study. Archives of Ophthalmology, 79(1), 28–30. [PubMed: 5635083]

Mashige K. (2013). A review of corneal diameter, curvature and thickness values and influencing factors. African Vision and Eye Health, 72(4), 185–194.

Massoudi D, Malecaze F, & Galiacy SD (2016). Collagens and proteoglycans of the cornea: Importance in transparency and visual disorders. Cell and Tissue Research, 363(2), 337–349. [PubMed: 26205093]

Nam SY, & Park S-H (2018). ECM based bioink for tissue mimetic 3D bioprinting (pp. 335–353). Biomimetic Medical Materials: Springer.

Noor N, Shapira A, Edri R, Gal I, Wertheim L, & Dvir T. (2019). 3D printing of personalized thick and perfusable cardiac patches and hearts. Advanced Science, 6, 1900344.

Ouyang L, Yao R, Chen X, Na J, & Sun W. (2015). 3D printing of HEK 293FT cell-laden hydrogel into macroporous constructs with high cell viability and normal biological functions. Biofabrication, 7(1), 015010. [PubMed: 25691496]

Pereira RF, Sousa A, Barrias CC, Bártolo PJ, & Granja PL (2018). A single-component hydrogel bioink for bioprinting of bioengineered 3D constructs for dermal tissue engineering. Materials Horizons, 5(6), 1100–1111.

Ramamurthy M, Lakshminarayanan V, Karlicek R, Sun C, Zissis G, & Ma R. (2015). Human vision and perception In Handbook of Advanced Lighting Technology (pp. 1–23). Springer International Publishing, Switzerland.

Sommer AC, & Blumenthal EZ (2019). Implementations of 3D printing in ophthalmology. Graefe's Archive for Clinical and Experimental Ophthalmology, 257, 1815–1822.

Sorbara L, Maram J, Fonn D, Woods C, & Simpson T. (2010). Metrics of the normal cornea: Anterior segment imaging with the Visante OCT. Clinical and Experimental Optometry, 93(3), 150–156. [PubMed: 20557556]

Tang MD, Golden AP, & Tien J. (2004). Fabrication of collagen gels that contain patterned, micrometer-scale cavities. Advanced Materials, 16(15), 1345–1348.

Van Best J, Bollemeijer J, & Sterk C. (1988). Corneal transmission in whole human eyes. Experimental Eye Research, 46(5), 765–768. [PubMed: 3384021]

Ventura AS, Böhnke M, & Mojon D. (2001). Central corneal thickness measurements in patients with normal tension glaucoma, primary open angle glaucoma, pseudoexfoliation glaucoma, or ocular hypertension. British Journal of Ophthalmology, 85(7), 792–795.

Wu Z, Su X, Xu Y, Kong B, Sun W, & Mi S. (2016). Bioprinting three-dimensional cell-laden tissue constructs with controllable degradation. Scientific Reports, 6, 24474. [PubMed: 27091175]

Young G. (1992). Ocular sagittal height and soft contact lens fit. Journal of the British Contact Lens Association, 15(1), 45–c49.

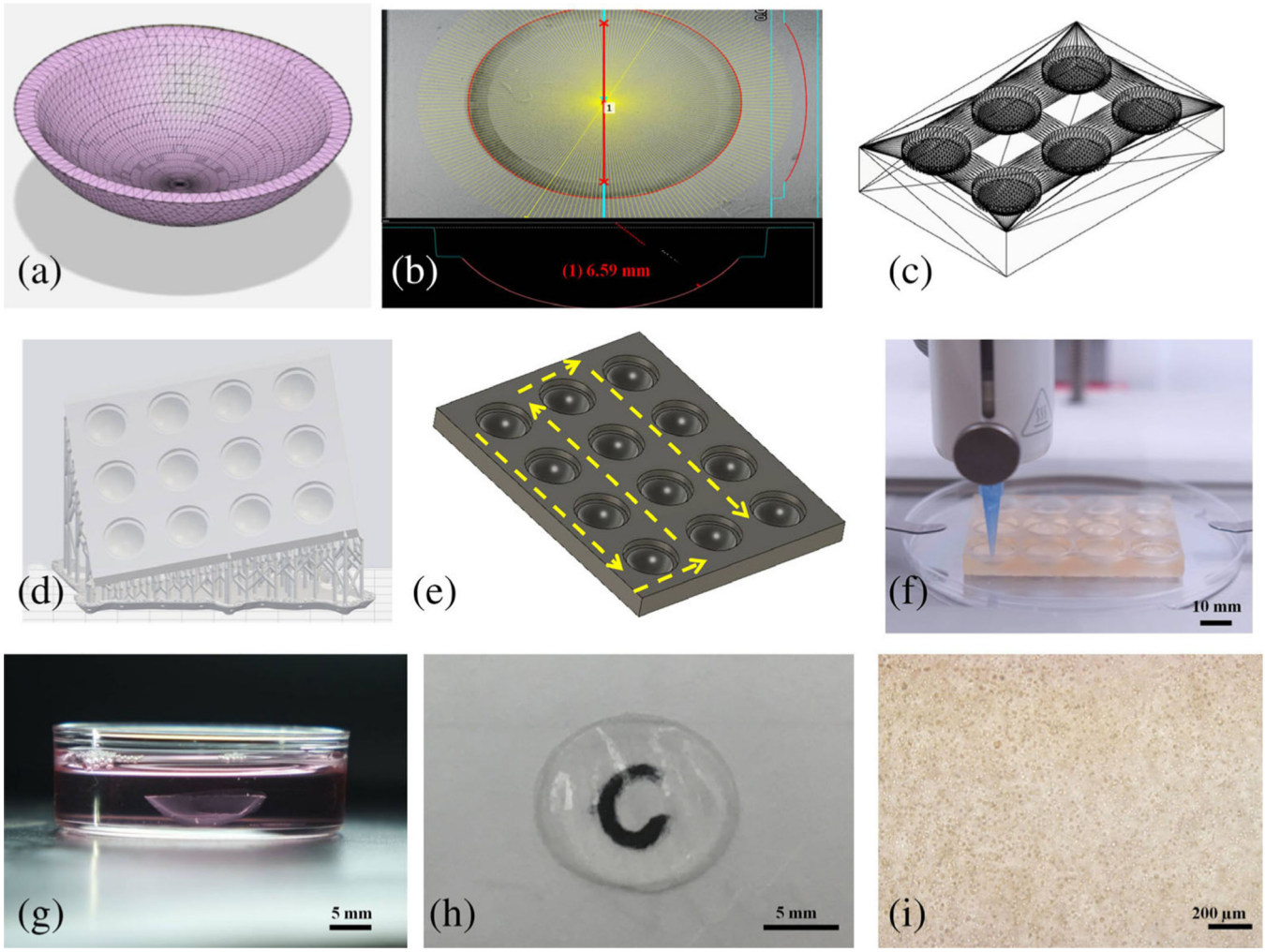

FIGURE 1.

The development of human corneal stroma and base support scaffolds apparatus. (a) Average corneal stroma dimensions modeled in Autodesk Fusion 360. (b) Bright-field image of single well of support scaffold showing its radius. (c) 3D model of 6-well corneal scaffold. (d) Support and raft preparation with Preform software for SLA printing of 12-well scaffold. (e) Printing path of 12-well corneal scaffold. (f) High-throughput printing of 12 corneas with a BIOX printer. (g) Printed cornea after crosslinking and placing within media. (h) Picture of cornea showing its transparency through the letter “C.” (i) Bright-field image of 3D printed cornea using inverted microscope on Day 1

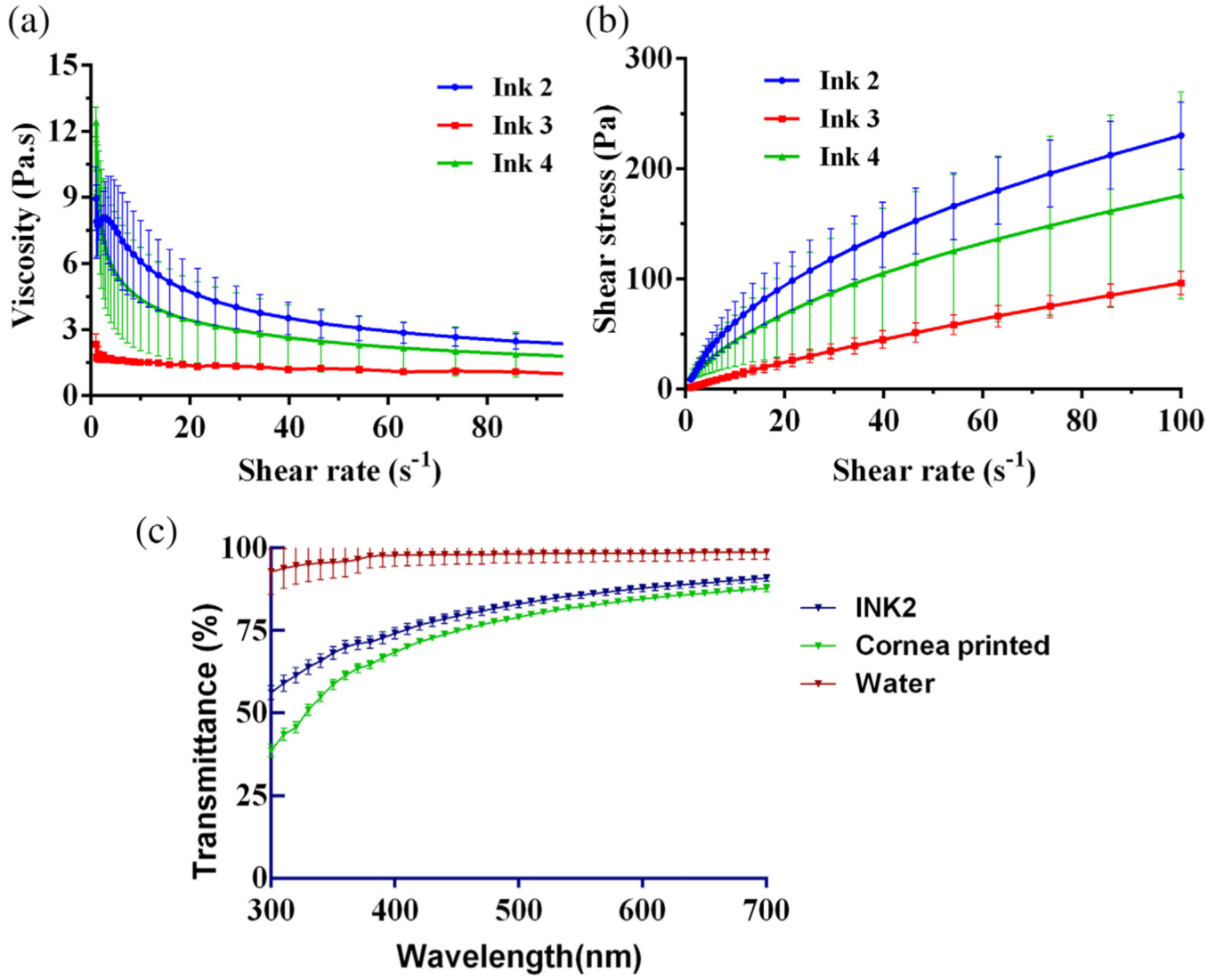

FIGURE 2.

Characterization of bioinks (a) Flow sweep test using rheometer to determine the viscosity at varying shear stress. Ink 2 exhibited higher viscosity as compared to others. (b) Shear stress vs shear rate behavior of bioinks showing shear thinning. (c) Light transmittance of bio-ink 2, 3D printed cornea at varying wavelengths compared with control (water)

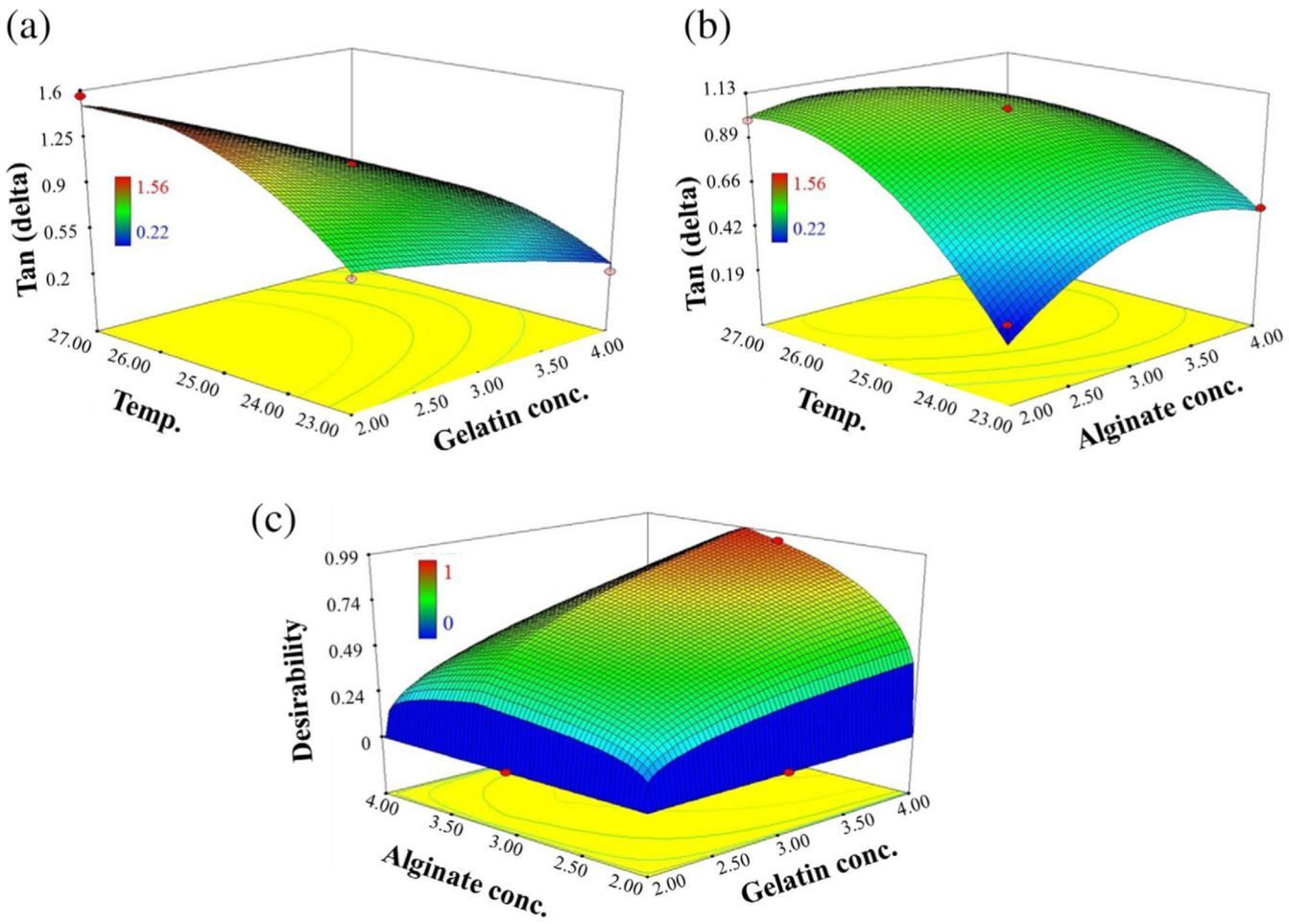

FIGURE 3.

Response 3D surface plots. (a) The effect of gelatin concentration and temperature on Tan (delta). Tan (delta) was significantly decreased on increase in gelatin concentration, whereas tan (delta) was significantly increased on increase in temperature. (b) The effect of alginate concentration and temperature on Tan (delta). Tan (delta) was significantly increased on increase in alginate concentration and temperature. (c) The selection of desired batch with low tan (delta) having maximum gelatin concentration, 3.25% alginate concentration, and temperature (23°C)

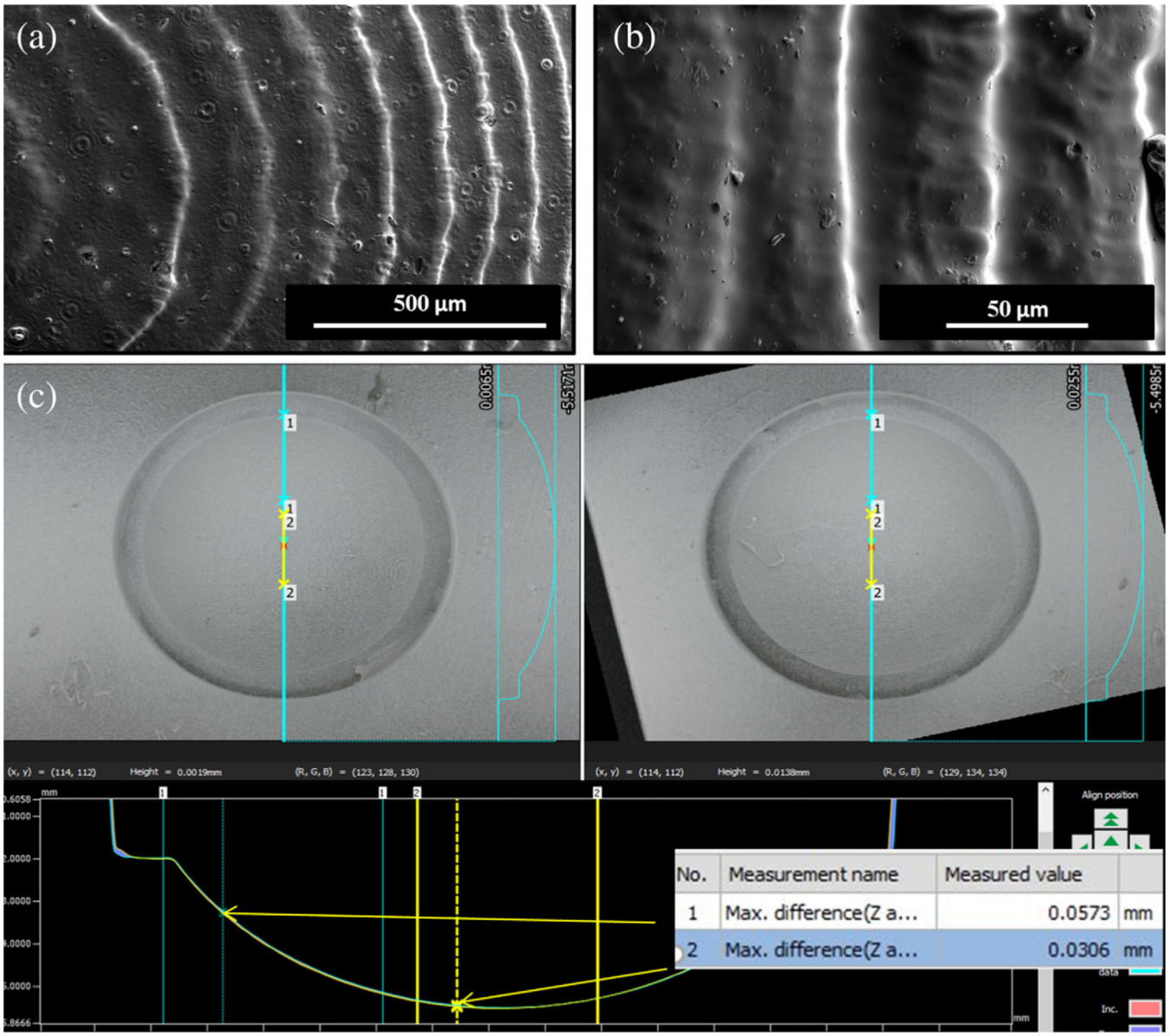

FIGURE 4.

Characterization of corneal support scaffold (a, b) SEM of PDMS corneas derived from support scaffold made of Dental SG Resin showing higher anterior surface resolution of SLA printed scaffold. (c) Brightfield images were captured for two different wells on the same scaffold to confirm the radius of the well and variation between two wells

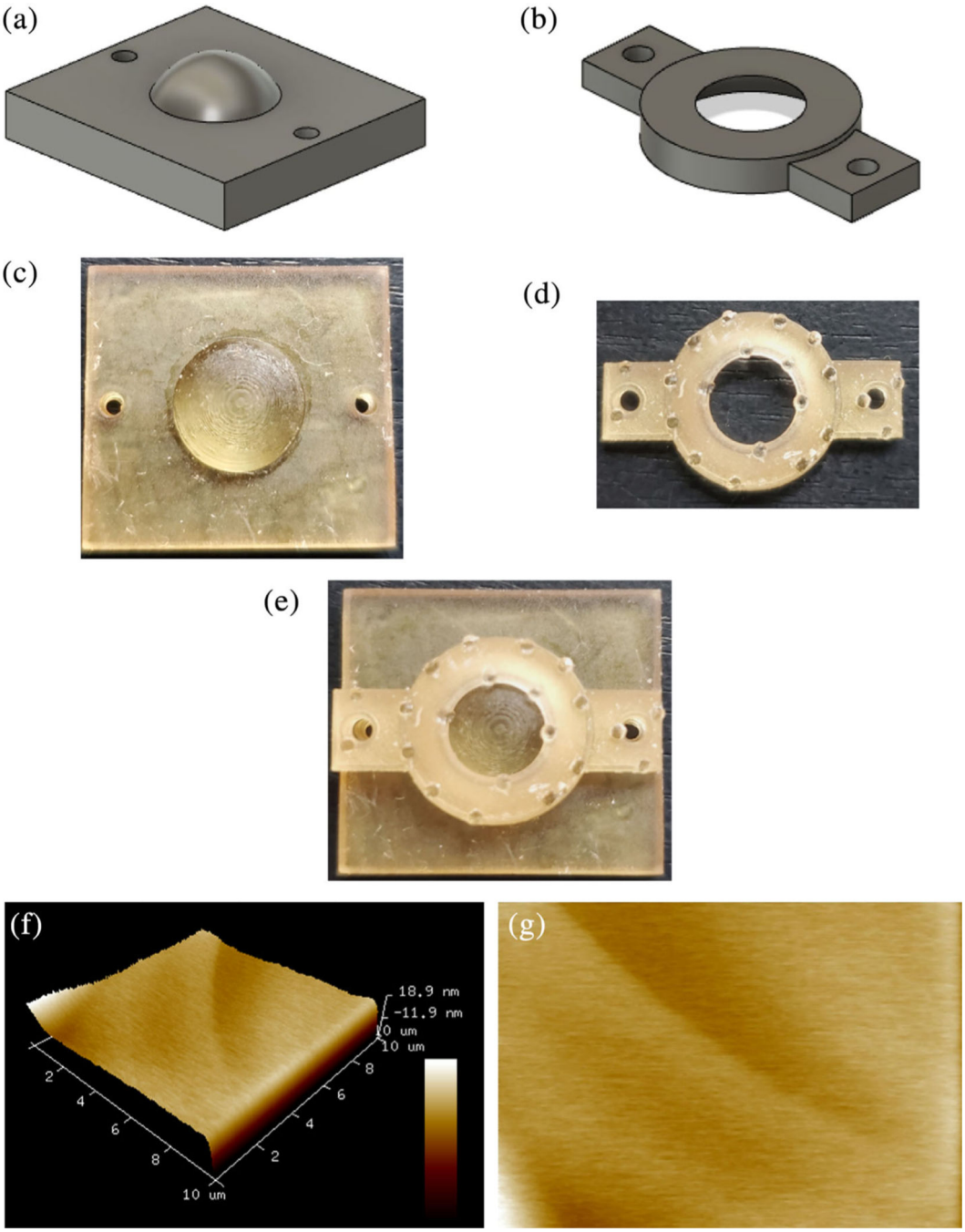

FIGURE 5.

3D printed cornea holder and AFM of 3D printed cornea (a) Side view of cornea seat (STL file) with dome in the center to securely place cornea. (b) Side view of cornea seat lid with hole to expose central region of cornea during AFM testing. (c) Top view SLA printed cornea seat. (d) Top view SLA printed cornea seat lid. (e) Top view of cornea holder securing cornea in the center anchored in place with the help of lid. (f) 3D printed corneal topography by atomic force microscopy over a scan area of 10 μm × 10 μm. (g) AFM image of 3D printed corneal stroma surface

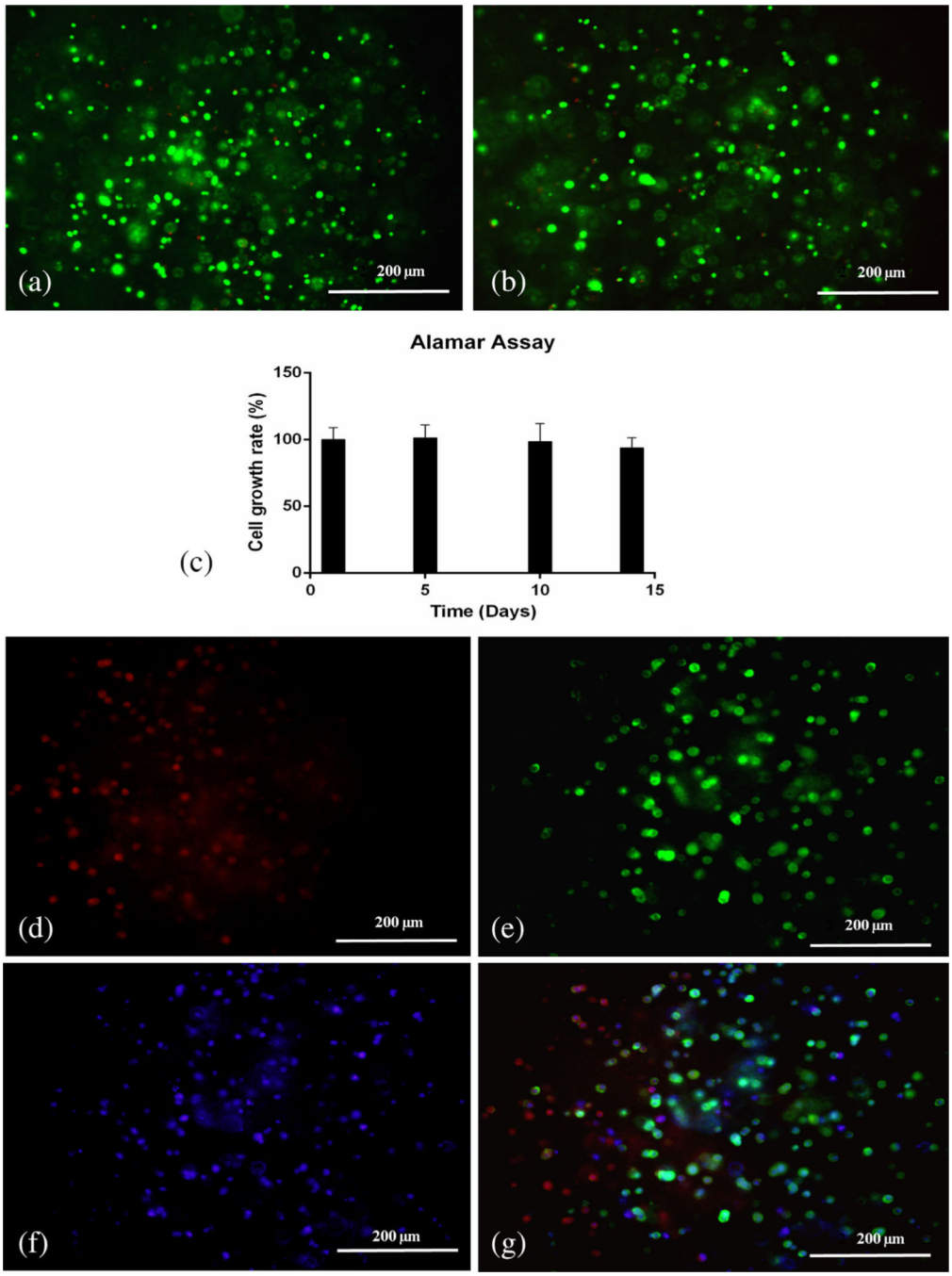

FIGURE 6.

Evaluation of cell viability and immunofluorescence staining of 3D bioprinted corneas. (a) Live dead assay in 3D printed corneas bearing human corneal keratocyte (HCK) cells on Day 1 (merged image). (b) Live dead assay in 3D printed corneas bearing HCK cells on Day 14 (merged image). (c) Alamar assay on 3D printed corneas on Days 1, 5, 10, and 14. Immunofluorescence staining of 3D printed corneas using a fluorescent microscope for (d) fibronectin (red), (e) F-actin (green), (f) DAPI (blue), and (g) merge image

TABLE 1

List of various bio-inks and their compositions formulated for quality by design analysis

Name	Gelatin (%)	Sodium alginate (%)	Collagen (mg/ml)
Ink 1	4.00	3.00	5.00
Ink 2	4.00	3.25	5.00
Ink 3	3.00	3.00	5.00
Ink 4	2.00	3.00	5.00
Ink 5	2.00	2.00	5.00
Ink 6	3.00	4.00	5.00
Ink 7	3.00	2.00	5.00
Ink 8	2.00	4.00	5.00
Ink 9	4.00	4.00	5.00
Ink 10	4.00	2.00	5.00

TABLE 2

Box–Behnken design of bio-inks

Run number	Gelatin (%)	Sodium alginate (%)	Temperature (°C)	Tan (delta)
1	4	3	23	0.22
2	3	4	23	0.53
3	2	2	25	1.15
4	2	3	27	l.56
5	4	3	27	0.51
6	3	3	25	1.05
7	3	4	27	0.5
8	3	3	25	1.05
9	3	2	27	0.99
10	2	4	25	1.17
11	4	4	25	0.46
12	3	3	25	1.05
13	3	3	25	1.05
14	4	2	25	0.4
15	2	3	23	0.71
16	3	3	25	1.05
17	3	2	23	0.29

TABLE 3

Analysis of variance for response surface quadratic model

Source	***p*-value**
Model	<.0001
A: Gelatin concentration	<.0001
B: Alginate concentration	.4633
C: Temperature	<.0001
AB	.8037
AC	.0086
BC	.0022
A^2	.3108
B^2	.0008
C^2	.0002

TABLE 4

Optimized batch selected based on constraints applied

Variables	Goal	Lower limit	Upper limit	Predicted optimized batch parameters
Optimization of bio-inks				
A: Gelatin concentration (%)	Maximize	2.00	4.00	4.00
B: Alginate concentration (%)	3.25	2.00	4.00	3.25
Temperature (°C)	Minimize	23	27	23

J Biomed Mater Res B Appl Biomater. Author manuscript; available in PMC 2021 January 05.